A01-34330

AIAA-2001-3638

Electromagnetic Effects in the Near Field Plume Exhaust of a Pulsed Plasma Thruster

Michael Keidar and Iain D. Boyd

University of Michigan, Ann Arbor MI 48109

37th AIAA/ASME/SAE/ASEE Joint Propulsion Conference and Exhibit

8-11 July 2001
Salt Lake City, Utah

AIAA-2001-3638

Electromagnetic Effects in the Near Field Plume Exhaust of a Pulsed Plasma Thruster

Michael Keidar[♦] and Iain D. Boyd*

University of Michigan, Ann Arbor, MI 48109

Abstract

In this work we present a model of the near field plasma plume of a Pulsed Plasma Thruster (PPT). As a working example we consider a micro-PPT developed at the Air Force Research Laboratory. This is a miniaturized design of the axisymmetric PPT with a thrust in the 10 μN range that utilizes Teflon™ as a propellant. The plasma plume is simulated using hybrid fluid-PIC-DSMC approach. The plasma plume model is combined with Teflon ablation and plasma generation models that provide boundary conditions for the plume. This approach provides a consistent description of the plasma flow from the surface into the near plume. The magnetic field diffusion into the plume region is also considered and plasma acceleration by the electromagnetic mechanism is studied. Teflon ablation and plasma generation analyses show that the Teflon surface temperature and plasma parameters are strongly non-uniform in the radial direction. The plasma density near the propellant surface peaks at about 10^{24} m^{-3} in the middle of the propellant face while the electron temperature peaks at about 4.5 eV near the electrodes. The model predicts ablated mass per pulse of about 1 μg that is close to that measured in experiment. The plume simulation shows that a dense plasma focus is developed at a few mm from the thruster exit plane at the axis. This plasma focus exists during the entire pulse, but the plasma density in the focus decreases from about 2×10^{22} m^{-3} at the beginning of the pulse down to 0.3×10^{22} m^{-3} at 5 μs. The velocity phase is centered at about 30 km/s in the axial direction. At later stages of the pulse there are two ion populations with positive and negative radial velocity. An ion population having negative axial velocity up to about 10 km/s is predicted. This is a significant finding in terms of backflow contamination onto a spacecraft.

♦ *Research Scientist, Department of Aerospace Engineering, Member of AIAA*

* *Associate Professor, Department of Aerospace Engineering, Senior Member of AIAA*

1. Introduction

The pulsed plasma thruster (PPT) was among the first of various electrical propulsion concepts accepted for space flight mainly due to its simplicity and hence high reliability[1]. However, the PPT has an efficiency that is generally low[2] at about 10% leaving open the opportunity for considerable improvement[3]. Currently, PPT's are considered as an attractive propulsion option for stationkeeping and drag makeup purposes of mass and power limited satellites[4,5]. Guaranteeing successful operation of spacecraft using a PPT requires a complete assessment of the spacecraft integration effects. The PPT plume contains various ion and neutral species due to propellant decomposition and possible electrode erosion. Some attempts of PPT plume modeling using particle simulations were performed recently[6,7,8]. In Refs. 7,8 we have considered the plume flowfield exhaust from an electrothermal PPT and therefore electromagnetic effects in the plume were neglected. Different variations of electromagnetic PPTs are also candidates for various missions[9]. Recently, a micro-PPT has being designed at AFRL for delivery of very small impulse bit[10]. This is a simplified miniaturized version of a conventional PPT designed to provide attitude control and stationkeeping for microsatellites. We will use the AFRL micro-PPT as a working example for several reasons. Firstly, electromagnetic ($j \times B$) acceleration is the primary mechanism in this thruster; and secondly, there is no internal flow in this device and therefore the near-field plasma plume is an essential part of the thrust generation process. Therefore careful modeling of the acceleration is needed to understand the characteristics of the device as a whole in addition to being a pre-cursor to accurate estimation of contamination issues. Since in this device there is no separation between the main plasma acceleration region and the plume expansion, both regions must be simulated in one model. Because the plasma acceleration is external, the plasma is sufficiently rarefied so that an MHD approach such as MACH2 (Ref. 11) cannot be used.

An accurate model of the PPT plume relies on the boundary and initial conditions. These conditions can be formulated by consideration of the Teflon ablation process. The Teflon ablation computation is based on a recently developed kinetic ablation model[12,13]. In this model the detailed physics of the Teflon evaporation is studied by consideration of the distribution function of the particles in the kinetic layer adjacent to the surface.

Another important effect related to the plasma plume exhaust from an electromagnetic PPT is the magnetic field diffusion into the near plume. Previously, we have modeled the effect of the magnetic field on the near-field plume for Hall thrusters[14] under steady state conditions. It was found that the magnitude of the magnetic field at the thruster exit has an important effect on the plasma potential distribution in the plume. In the present research, it is proposed to include the electromagnetic effects on the near field plume of unsteady plasma flow. The computational domain is shown in Fig. 1. The model is based on a hybrid approach involving a DSMC description of neutrals, a PIC model for ions and a fluid description of the electrons. In these methods, the potential distribution is usually calculated by reducing the electron momentum equation to the Boltzmann relation in the absence of a magnetic field. In the plasma plume domain where the magnetic field exists, i.e. the near field, it is necessary to include the magnetic field effects in the electron momentum equation.

2. The model of the plasma layer

The model presented here describes the plasma layer near the Teflon surface as shown in Fig. 2. The model of the plasma layer includes Joule heating of the plasma, heat transfer to the Teflon, and Teflon ablation. Mechanisms of energy transfer from the plasma column to the wall of the Teflon include heat transfer by particle convection and by radiation. The Teflon ablation computation is based on a recently developed kinetic ablation model[12]. It is assumed that within

the plasma layer all parameters vary in the radial direction r (see Fig. 2). The energy balance equation can be written in the form:

$$\frac{3}{2} n_e \, dT_e/dt = Q_J - Q_r - Q_F \quad (1)$$

where Q_J is the Joule heat, Q_r is the radiation heat and Q_F is the heat associated with particle fluxes. This equation depends on the coordinate along the propellant face. For known plasma density and temperature the heat flux to the surface is calculated. The Teflon surface temperature is calculated from the heat transfer equation with boundary conditions that take into account vaporization heat and conductivity. The solution of this equation is considered for two limiting cases of substantial and small ablation rate very similar to that described in Ref. 8. The density at the Teflon surface is calculated using the equilibrium pressure for Teflon. The plasma density in the layer is determined in the framework of the kinetic ablation model (see next section). For known pressure and electron temperature one can calculate the chemical plasma composition assuming LTE[8,15,16]. The Saha equations are supplemented by the conservation of nuclei and quasi-neutrality.

3. Ablation model

The Teflon ablation is modeled in the framework of the approximation[13] based on a kinetic model of the material evaporation into discharge plasmas[12]. The model couples two different layers between the surface and the plasma bulk as shown in Fig. 2b: (1) a kinetic non-equilibrium layer adjusted to the surface with a thickness of about one mean free path; and (2) a collision-dominated layer with thermal and ionization non-equilibrium. The velocity at the edge of the kinetic layer U_1 can be determined from the coupling solution of the hydrodynamic layer and the

quasi-neutral plasma. For known velocity and density at this interface, it is possible to calculate the ablation rate. In the hydrodynamic layer the relation between the velocities, temperatures and densities at the boundaries 1 and 2 as well as the ablation rate are formulated according to Ref. 13 in the form:

$$\Gamma = mU_1N_1 = N_1[(2kT_1/m)\cdot(T_2N_2/2T_1 - N_1/2)/(N_1 - N_1^2/N_2)]^{0.5} \quad \text{.....(2)}$$

The system of equations is closed if the equilibrium vapor pressure can be specified that determines parameters (N_o and T_o) at the Teflon surface. The full self-consistent solution of this problem can be obtained when the ablation is coupled with the plasma plume expansion. In the present work in order to simplify the problem, we will assume that the plasma accelerates up to the sound speed near the boundary 2. This assumption can be justified by the fact that due to significant electrodynamic acceleration in this type of PPT, the plasma density will quickly decrease therefore providing solution of the ablation problem close to that ablation into the vacuum. In this case the plasma density at the edge of the kinetic layer will be equal to $0.34\cdot N_o$ and the temperature is $0.7\cdot T_o$. The flux returned to the surface is equal to 16% of the ablated flux (Ref. 12).

4. Plasma plume electrodynamics

The general approach for the plume model is based on a hybrid fluid-particle approach that was used previously (Refs. 7). In this model, the neutrals and ions are modeled as particles while electrons are treated as a fluid. Elastic (momentum transfer) and non-elastic (charge exchange) collisions are included in the model. The grids employed in this computation are also similar to those used previously (Ref.7). The particle collisions are calculated using the direct simulation

Monte Carlo (DSMC) method[17]. Momentum exchange cross sections use the model of Dalgarno et al.[18], while charge exchange processes use the cross sections proposed by Sakabe and Izawa[19]. Acceleration of the charged particles is computed using the Particle-In-Cell method (PIC)[20]. The plasma velocity distribution depends upon the magnetic field distribution and ion dynamics is calculated as follows:

$$d\mathbf{V}/dr = -C_s^2 \nabla \ln(n) + \mathbf{j} \times \mathbf{B}/mn \quad (3)$$

where C_s is the sound speed, n is the plasma density, j is the current density and B is the magnetic field.

The electron dynamics is very important in the plasma plume. Previously our model was based on the assumption that electrons rapidly reach the equilibrium distribution and in the absence of the magnetic field can be described according to the Boltzmann distribution. While this was a satisfactory assumption in the case of an electrothermal thruster plume this is not suitable for the near field of an electromagnetic thruster. In the presence of a strong magnetic field, the electron density distribution deviates from that according to Boltzmann[21]. In the case of a magnetic field the electron momentum equation reads (neglecting electron inertia):

$$0 = -e^2 n_e(\mathbf{E}+\mathbf{V}_e \times \mathbf{B}) - e\nabla P_e - \nu_{ei} m_e \mathbf{j} \quad (4)$$

We have assumed quasi-neutrality therefore $n_e = n_I = n$. The electric and magnetic field distributions in the plume are calculated from the set of Maxwell equations. We further assume that the magnetic field has only an azimuthal component and also neglect the displacement

current. The combination of the Maxwell equations and electron momentum conservation gives the following equation for the magnetic field:

$$\partial \mathbf{B}/\partial t = 1/(\sigma\mu)\nabla^2\mathbf{B} - \nabla\times(\mathbf{j}\times\mathbf{B}/(en)) + \nabla\times(\mathbf{V}\times\mathbf{B}) \quad (5)$$

where σ is the plasma conductivity, μ is the permittivity, n is the plasma density, **j** is the current density and **V** is the plasma velocity. A scaling analysis shows that the various terms on the right hand side of Eq. 5 may have importance in different regions of the plasma plume and therefore general end-to-end plasma plume analysis requires keeping all terms in the equation. In the case of the near plume of the micro-PPT with a characteristic scale length of about 1 cm the magnetic Reynolds number $Re_m<<1$ and therefore the last term can be neglected. Taking this into account in the dimensionless form, Eq. 5 can be written as:

$$Re_m \frac{\partial B}{\partial t} = \nabla^2 B - (\omega\tau)\cdot\{\frac{\partial}{\partial r}(\frac{Br}{r\cdot n})\frac{\partial(Br)}{\partial z} - \frac{\partial}{\partial z}(\frac{Br}{r\cdot n})\frac{\partial(Br)}{\partial r}\} \quad (6)$$

where $(\omega\tau)$ is the Hall parameter that measures of the Hall effect. Therefore, depending on the plasma density, the Hall effect may be important for the magnetic field evolution. One of the first calculations of the plasma flow with Hall effect were performed by Brushlinski and Morozov (see Ref. 22 and references therein). They considered isothermal flow. The plasma density becomes high at the cathode and lower at the anode. The Hall effect has a particularly noticeable influence on the magnetic field distribution. The field near the anode increases and near the cathode decreases. As a result the current is deflected to the side and grazes the anode.

Our estimations show that the Hall parameter $\omega\tau<<1$ if the plasma density near the Teflon surface $N>10^{23}$ m^{-3}. This case is realized in the micro-PPT (see the next section) so the Hall effect is

expected to be small for this particular case. Having the magnetic field distribution one can calculate the current density distribution from Ampere's law:

$$\mu \mathbf{j} = \nabla \mathrm{x} \mathbf{B} \quad \ldots\ldots (7)$$

The magnetic field and current distributions calculated from this model are used in PIC to evaluate the ion dynamics according to Eq. 3.

5. Boundary conditions

The boundary conditions for the magnetic field calculations are shown in Fig. 1. We have assumed that the current is uniform on both electrodes that allows us to estimate the current density on the cathode j_c and on the anode j_a. The magnetic field is assumed to vary as 1/r on the upstream boundary. At the lateral boundary we have assumed that the normal current j_n=0. The downstream boundary is considered to be far enough away that B=0 can be assumed. Along the centerline the magnetic field B=0.

The boundary conditions for the plume are generated through solution of the Teflon ablation problem as will be presented in the Results section. These are time and radial dependent variations of the plasma (including Carbon and Flourine ions and neutrals) density and electron temperature.

The results are presented for a 3.6 mm diameter micro-PPT which has a 0.9 mm diameter central electrode, 3.1 mm propellant diameter and 0.24 mm anode wall (Ref. 10). In these simulations,

the experimental current waveform was used, that is described in a first approximation as an underdamped LRC circuit current:

$$I(t) = I_p \cdot \sin(\alpha t)\exp(-\beta t)$$

where $I_p = \sqrt{\frac{2E}{L}}$; $\alpha = \sqrt{\frac{1}{LC}}$; $\beta = \frac{R}{2L}$; L is the effective inductance in the circuit, C is the capacitance, R is the total circuit resistance, and E is the pulse energy. The best fit with the experimental waveform (frequency) corresponds to $\alpha = 3 \cdot 10^6$ s^{-1}. For C=0.3 μF we can estimate that L in the circuit is about $3.6 \cdot 10^{-7}$ H. Results presented below correspond to the 15.2 J (Ref.10).

6. Results

The spatial and temporal variation of the Teflon surface temperature is shown in Fig. 3a. The Teflon temperature sharply increases during the first 1-2 μs of the pulse and peaks at about 635 K. One can see that the temperature is generally non-uniform in the radial direction and has a minimum at radial distances of 1.1-1.3 mm. Since the Teflon ablation is approximately exponentially proportional to the surface temperature, the model predicts a lower rate of ablation in the areas where the surface temperature has a minimum. Taking this into account, the effect of the temperature distribution may be related to the preferential charring of the Teflon surface observed experimentally [Ref. 10]. A detailed study of the Teflon surface charring and its relation to the non-uniform ablation will be presented in a parallel paper [23].

The plasma density and electron temperature distribution are also shown in Fig. 3. The plasma density peaks at about 10^{24} m^{-3} midway between the electrodes. The electron temperature is strongly non-uniform radially with peak near the electrodes of about 4.5 eV. The reason for

higher electron temperature near the electrodes is due to current spreading in the space between the electrodes and current focusing near the electrodes (see below results on current distribution). As was mentioned earlier, the ablation rate is also non-uniform radially. This effect is shown in Fig. 4. One can see that the ablation rate peaks near the electrodes at about 120 kg/m^{2}s, while in the middle of the propellant face it is about 80-100 kg/m^{2}s. The calculated total ablated mass per pulse was about 1 μg that is close to the measured value of 1.3 μg [10].

A region of magnetic field diffusion in the near field outside the micro-PPT is shown in Fig. 5a. The magnetic field drops by an order of magnitude at about 1.5 mm that is equal to the thruster radius. This is the region where also the most of the current is concentrated as shown in Fig. 5b. One can see that the current density is high near the central electrode and near the outer electrode. This is a reason for the increasing Teflon surface temperature and electron temperature in these regions. According to the model presented in Sec. 4 the electromagnetic acceleration of the plasma is also expected to occur in this region.

Figure 6 shows evolution of the Carbon ion (C+) component of the plasma plume during the main part of the pulse. One can see that a dense plasma focus is developed at a few mm from the thruster exit plane. This plasma focus exists during the entire pulse as shown in Fig. 6, but the plasma density in the focus decreases from about 2×10^{22} m^{-3} at the beginning of the pulse down to 0.3×10^{22} m^{-3} at 5 μs. At the beginning (first 2 μs) the C+ density mainly develops a gradient in the radial direction that is a result of high directed velocity in the axial direction. Later, during the pulse, the axial density gradient becomes comparable to the radial one.

The Flourine ions (F+), due to their larger mass, have different dynamics as shown in Fig.7. They have smaller acceleration in the axial direction even at the beginning of the pulse and therefore

both axial and radial density gradients are developed. The F+ density in the plume and in the plasma focus is larger than that of C+, because originally Teflon has composition C_2F_4 with F density twice larger than that of C. Additionally F ions experience less acceleration in the plume because of their mass that also contribute to their relative density increase.

The micro-PPT is essentially an electromagnetic accelerator as shown in the velocity phase plots (Figs. 8,9). The phase plot of the Carbon ions at 1 μs is centered at 30 km/s in the axial direction. Ions experience also radial expansion in both directions due to the magnetic field structure and the temperature expansion. The radial velocity in the negative direction is related to the focus formation along the axis, as shown in Figs. 6,7. The Flourine ions have generally smaller both axial and radial velocities due to their higher mass. At a later stage of the pulse (see Fig. 9) clearly there are two ion populations with positive and negative radial velocities. This is due to the annular plasma injection corresponding to the thruster geometry (see Figs. 1,2).

During the entire pulse there is a population of ions having a negative axial velocity with the magnitude up to about 10 km/s (see Figs. 8,9). This population creates the backflow contamination that is an important issue of concern for a spacecraft using the PPT. The Carbon ions have a larger negative velocity due to their higher mobility that results in their domination in the backflux.

7. Summary

In this paper, a self-consistent description of an electromagnetic pulsed plasma thruster from plasma generation into the near plume is presented. A micro-PPT developed at AFRL is considered as a working example. In this device, no separation exists between the main plasma acceleration region, which usually occurs in an internal flow, and the external plasma plume field. Therefore, a single end-to-end model is necessary for accurate simulations. A kinetic Teflon ablation model is incorporated in order to provide the boundary conditions for the plasma plume. This model predicts an ablated mass per pulse of about 1 μg that is close to that measured in experiment. The phenomena in the plasma plume related to the electromagnetic effects are studied. The plume simulation shows that a dense plasma focus is developed at a few millimeters from the thruster exit plane at the axis. This plasma focus exists during the entire pulse, but the plasma density in the focus decreases from about 2×10^{22} m^{-3} at the beginning of the pulse down 0.3×10^{22} m^{-3} at 5 μs. The velocity phase is centered at about 30 km/s in the axial direction demonstrating that the micro-PPT is essentially an electromagnetic accelerator. At a later stage of the pulse there are two ion populations with positive and negative radial velocity. It is predicted that there is a population of ions having a negative axial velocity magnitude up to about 10 km/s. This population relates to the backflow contamination that is an important issue of concern for a spacecraft using the PPT.

Acknowledgements

The authors gratefully acknowledge financial support by the Air Force Office of Scientific Research through grant F49620-99-1-0040. We also acknowledge Drs. Greg. G. Spanjers and Frank Gulczinski for valuable discussions and for providing the experimental data.

REFERENCES

[1] R. L. Burton and P. J. Turchi, "Pulsed plasma thruster", Journal of Propulsion and Power, Vol.14, No. 5, 1998, pp. 716-735.

[2] R.J. Vondra and K.I. Thomassen, "Flight qualified pulsed plasma thruster for satellite control", *Journal of Spacecraft and Rockets*, Vol. 11, No. 9, 1974, pp. 613-617.

[3] P. J. Turchi, Directions for improving PPT performance, *Proceeding of the 25th International Electric Propulsion Conference*, vol. 1, Worthington, OH, 1998, pp. 251-258.

[4]E. Y. Choueiri, "System optimization of ablative pulsed plasma thruster for stationkeeping", *Journal of Spacecraft and Rockets*, Vol. 33, No. 1, 1996, pp. 96-100.

[5]R. A. Spores, R. B. Cohen and M. Birkan, "The USAF Electric propulsion program", *Proceeding of the 25th International Electric Propulsion Conference*, vol. 1, Worthington, OH, 1998, 1997, p.1.

[6] N. A. Gatsonis and X. Yin, Axisymmetric DSMC/PIC simulation of quasineutral partially ionized jets, AIAA paper 97-2535, 1997.

[7] I. D. Boyd, M. Keidar, and W. McKeon, Modeling of a pulsed plasma thruster from plasma generation to plume far field, *Journal of Spacecraft and Rockets, Vol. 37, No. 3, 2000.*

[8] M. Keidar and I.D. Boyd, "Device and plume model of an electrothermal pulsed plasma thruster", Paper AIAA-2000-3430.

[9] W.A. Hoskins and R.J. Cassady, " Applications for Pulsed Plasma Thrusters and the Development of Small PPTs for Microspacecraft", AIAA-2000-3434.

[10] F. Gulczinski III, M. Dulligan, J. Lakes and G. Spanjers, "Micropropulsion research at AFRL", Paper AIAA-2000-3255

[11] P.G. Mikellides and P. J. Turchi, "Modeling of late-time ablation in Teflon pulsed plasma thruster", AIAA Paper 96-2733.

[12] M. Keidar, J. Fan, I.D. Boyd and I.I. Beilis, "Vaporization of heated materials into discharge plasmas", J. Appl. Phys., 89, 2001, pp. 3095-3098.

[13] M. Keidar, I.D. Boyd and I.I. Beilis, "On the model of Teflon ablation in an ablation-controlled discharge", J. Phys. D: Appl. Phys., 34, June, 2001, pp. 1675-1677.

[14] M. Keidar and I.D. Boyd, Effect of a magnetic field on the plasma plume from Hall thruster, *J. Appl. Phys.*, 86, 1999, pp. 4786-4791.

[15] P. Kovatya, Thermodynamic and transport properties of ablated vapors of PTFE, alumina, perspex and PVC in the temperature range 5000-30000 K, IEEE Trans. Plasma Sci., 12, 1984 pp. 38-42.

[16] C.S. Schmahl and P.J. Turchi, Development of equation-of-state and transport properties for molecular plasmas in pulsed plasma thrusters. Part I: A two-temperature equation of state for Teflon, Proc. Inter. Electr. Propul. Conf. Pp. 781-788, 1997.

[17] G.A. Bird, *"Molecular gas dynamics and the direct simulation of gas flows"* (Clarendon Press, Oxford, 1994).

[18] A. Dalgarno, M.R.C. McDowell and A. Williams, The modilities of ions in unlike gases, Proc. Of Royal Soc. Of London, Vol. 250, April 1958, pp. 411-425.

[19] S. Sakabe and Y. Izawa, Simple formula for the cross sections of resonant charge transfer between atoms and their ions at low impact velocity, Physical Rev. A: General Physics, v. 45, No. 3, 1992, pp. 2086-2089.

[20] C.K. Birdsall and A.B. Langdon, Plasma Physics via Computer Simulation, Adam Hilger Press, 1991.

[21] I.I. Beilis, M. Keidar and S. Goldsmith, "Plasma-wall transition: The influence of the electron to ion current ratio on the magnetic presheath structure", Phys. Plasmas, 4, 1997, pp. 3461-3468.

[22] K.V. Brushlinskii ans A.I. Morozov, "Calculation of two-dimensional plasma flows in channels", in Rev. Plasma Physics, Ed. M.A. Leontovich, Volume 8, 1980, Consultants Bureau, New York.

[23] M. Keidar, I.D. Boyd, F. Gulczinski III and G.G. Spanjers, "Analyses of Teflon surface charring in a micro-Pulsed Plasma Thruster", to be presented at *27th International Electric Propulsion Conference*, IEPC-01-155.

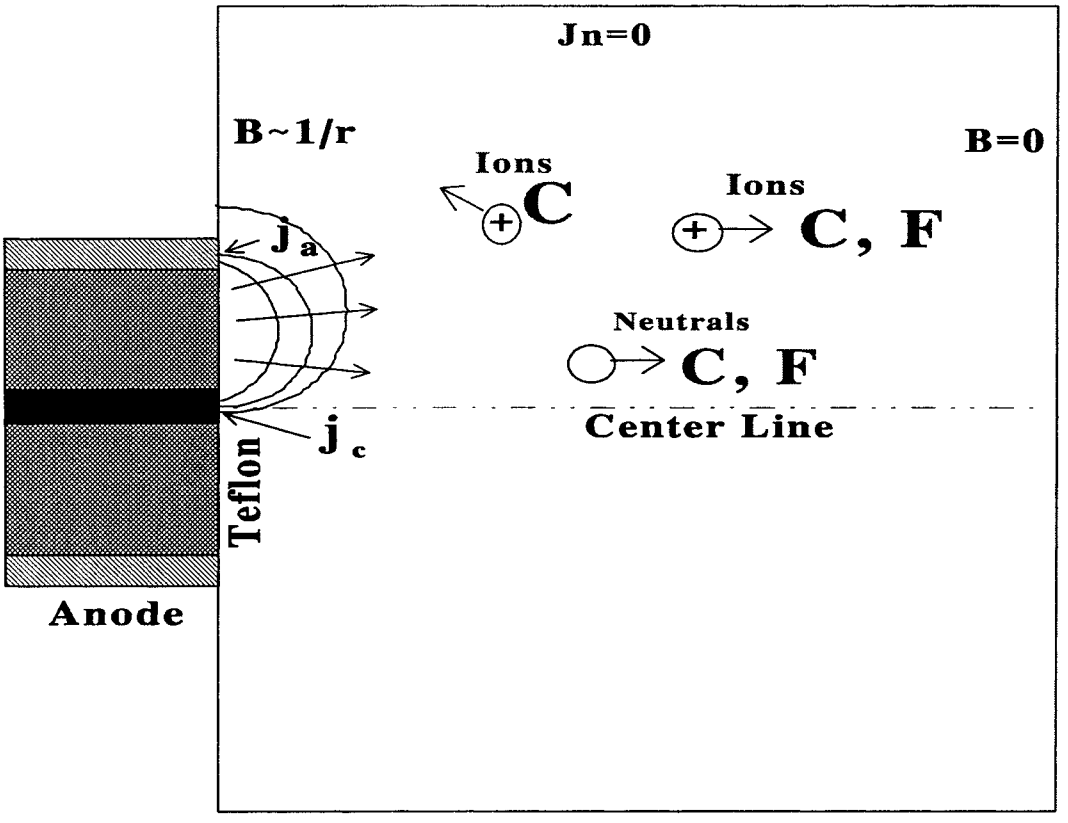

Figure 1. Schematic diagram of micro-PPT plume and boundary conditions

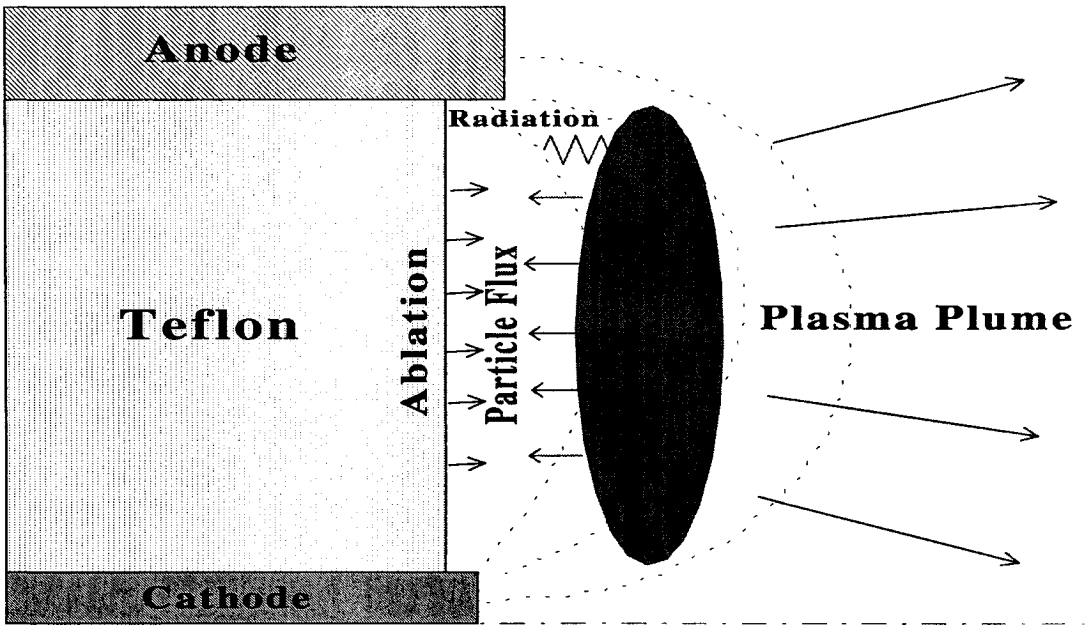

(a)

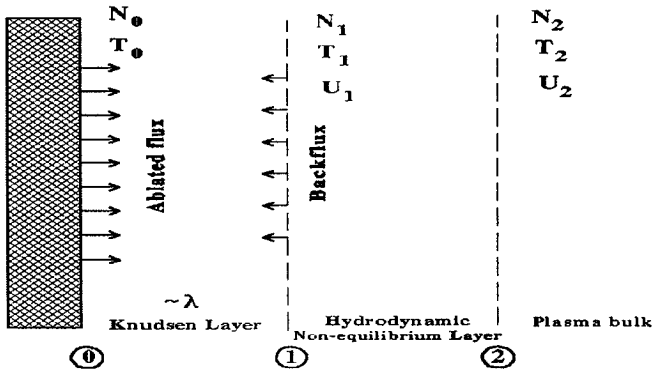

(b)

Figure 2. Schematic of the near Teflon plasma layer

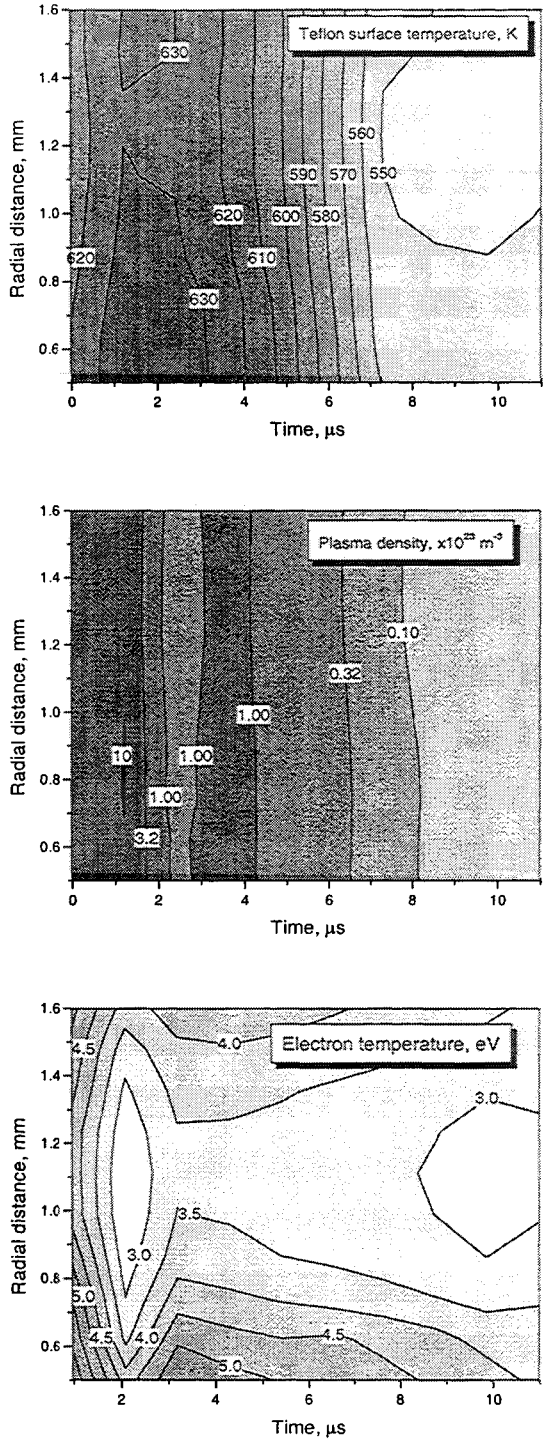

Figure 3. Teflon surface temperature, plasma density and elecrtron temperature distribution in the layer near the Teflon surface

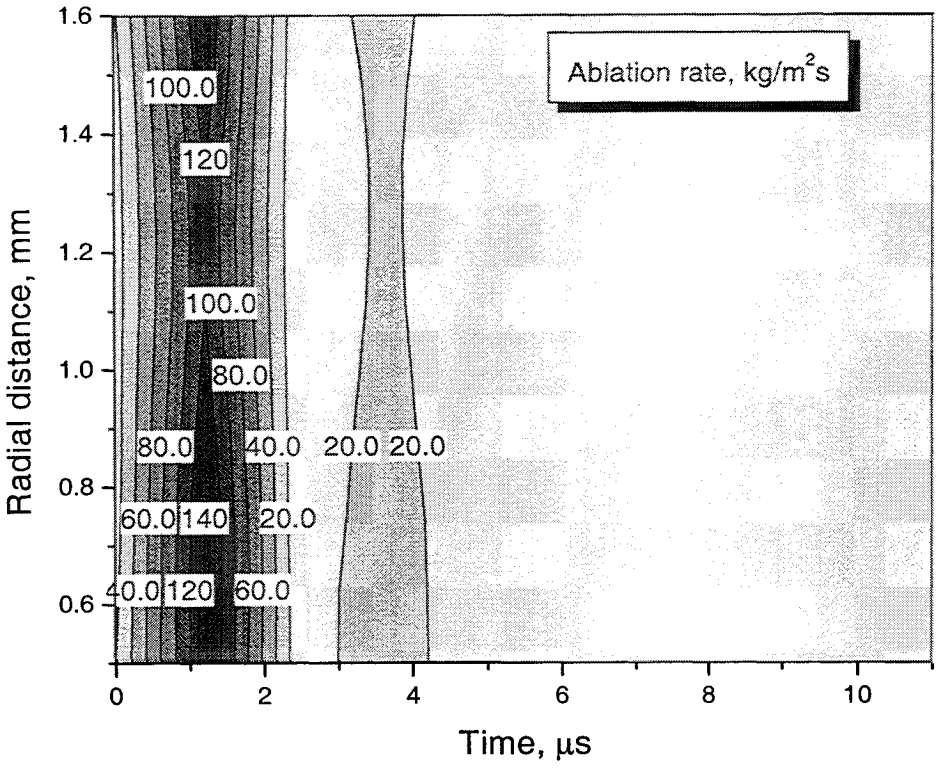

Figure 4. Ablation rate spatial and temporal distribution.

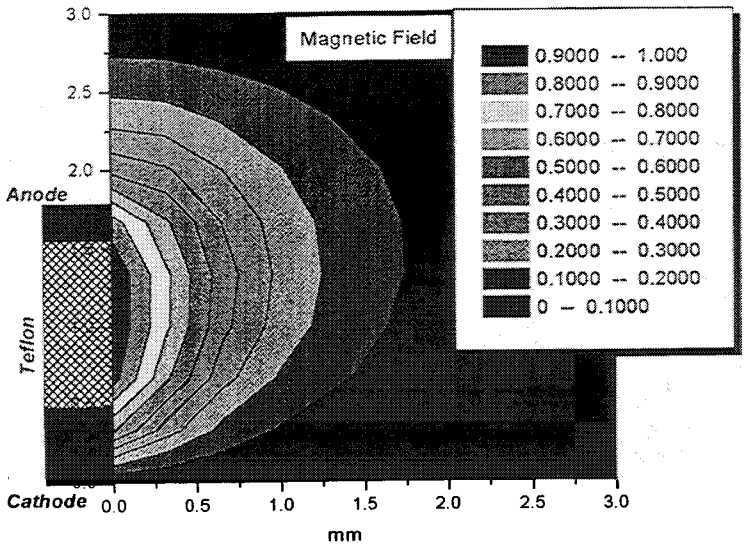

(a)

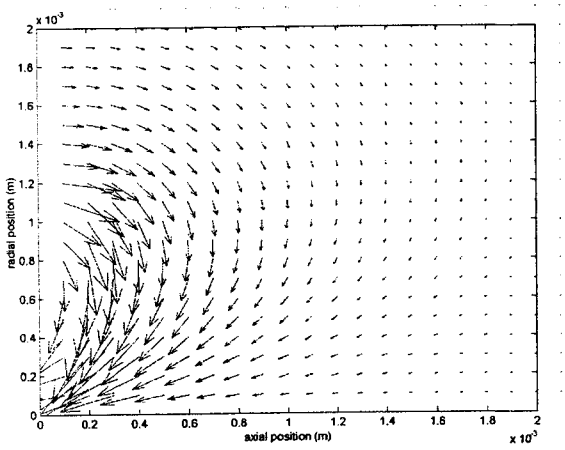

(b)

Figure 5. (a) Magnetic field distribution and (b) current lines vectors in the near field of the micro-PPT.

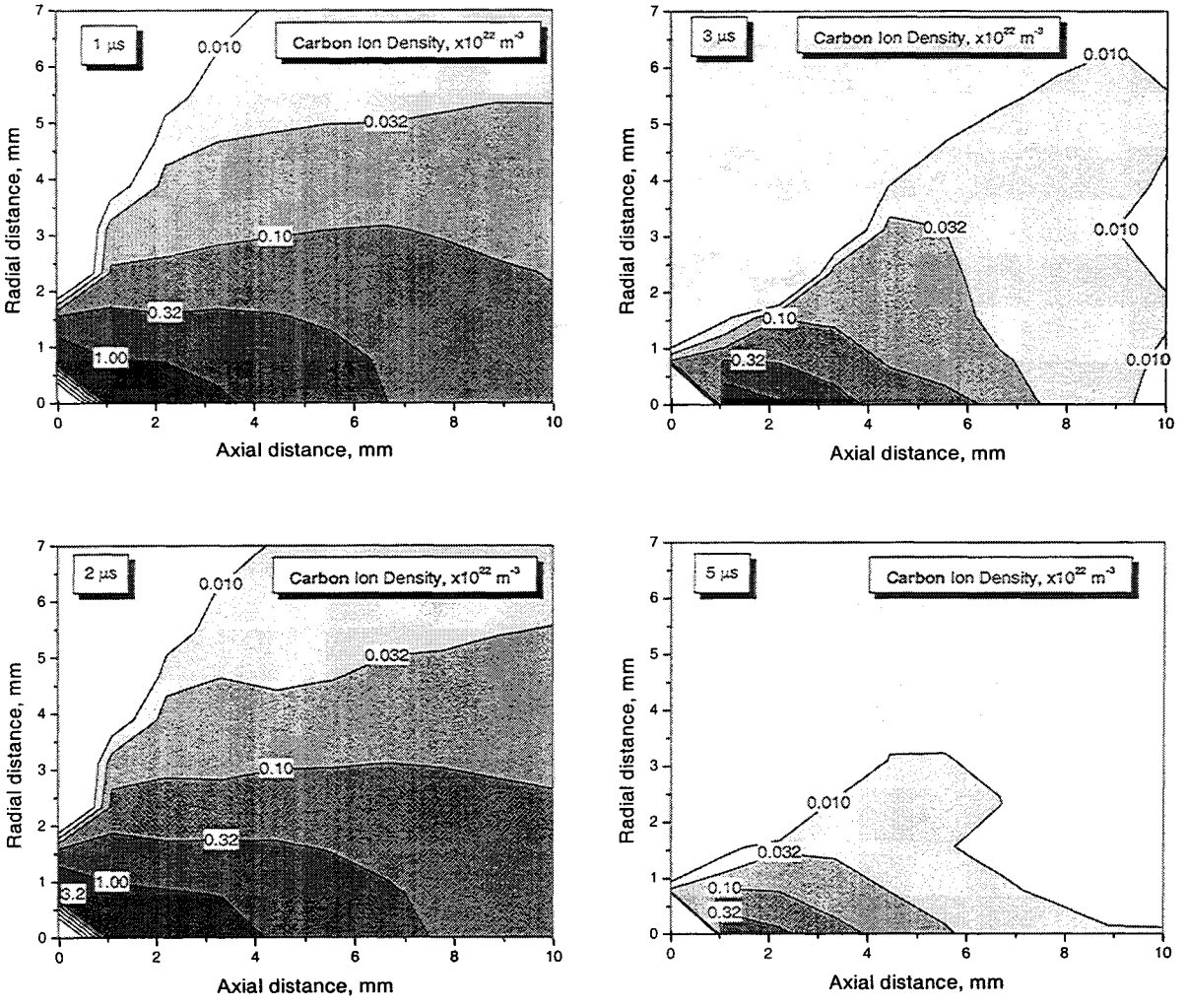

Figure 6. Evolution of the Carbon ion density during the pulse

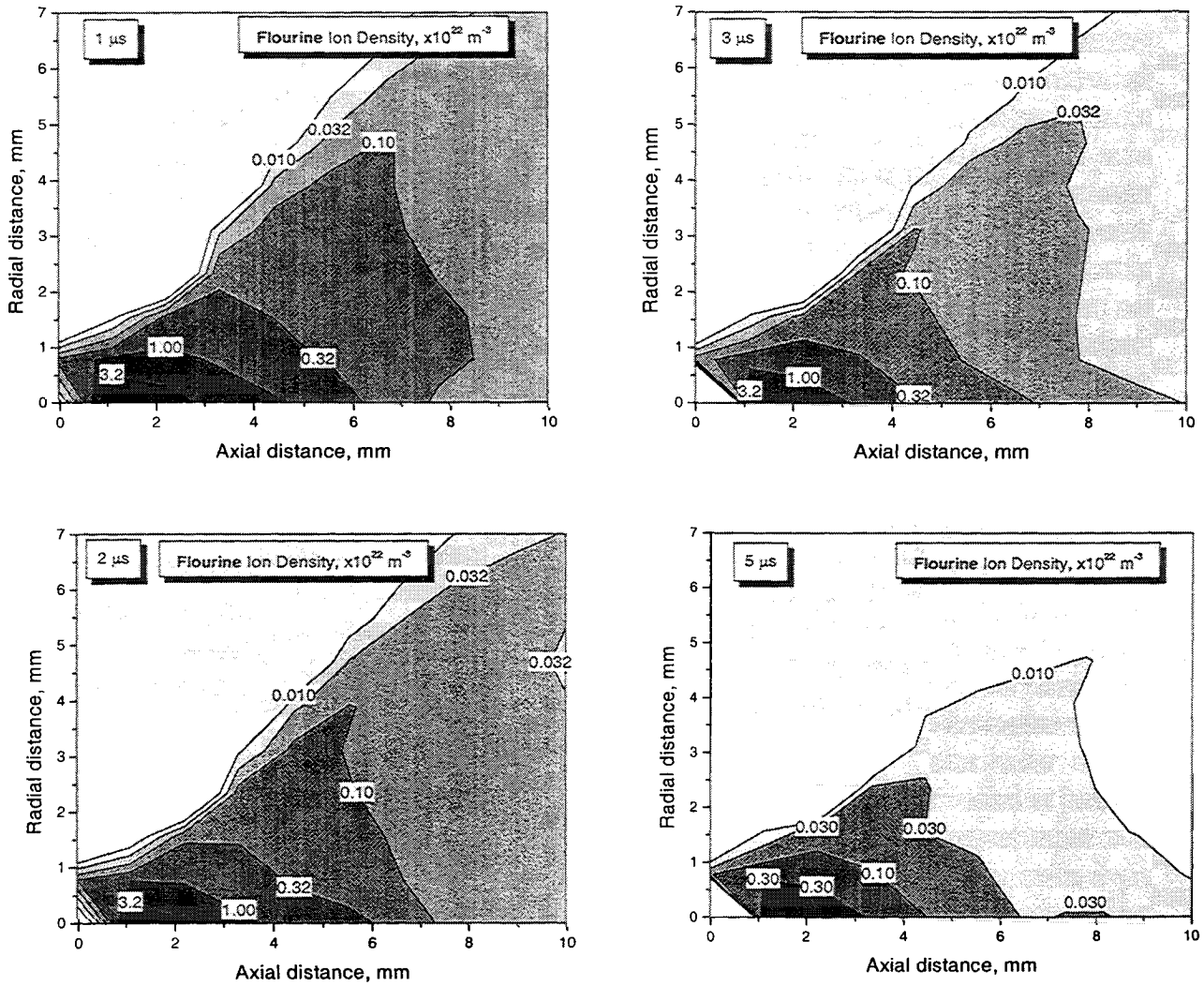

Figure 7. Evolution of the Flourine ion density during the pulse

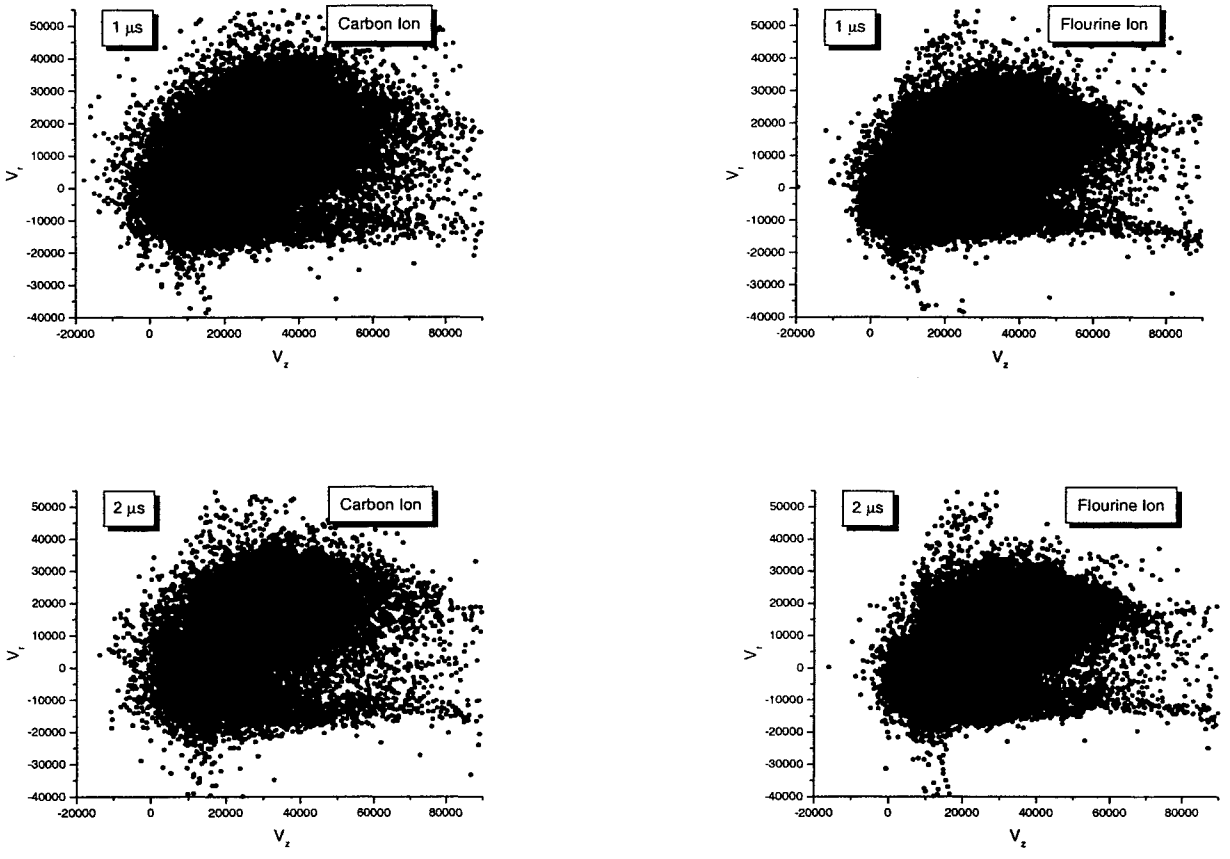

Figure 8. Ion velocity phase. Early stage of the pulse

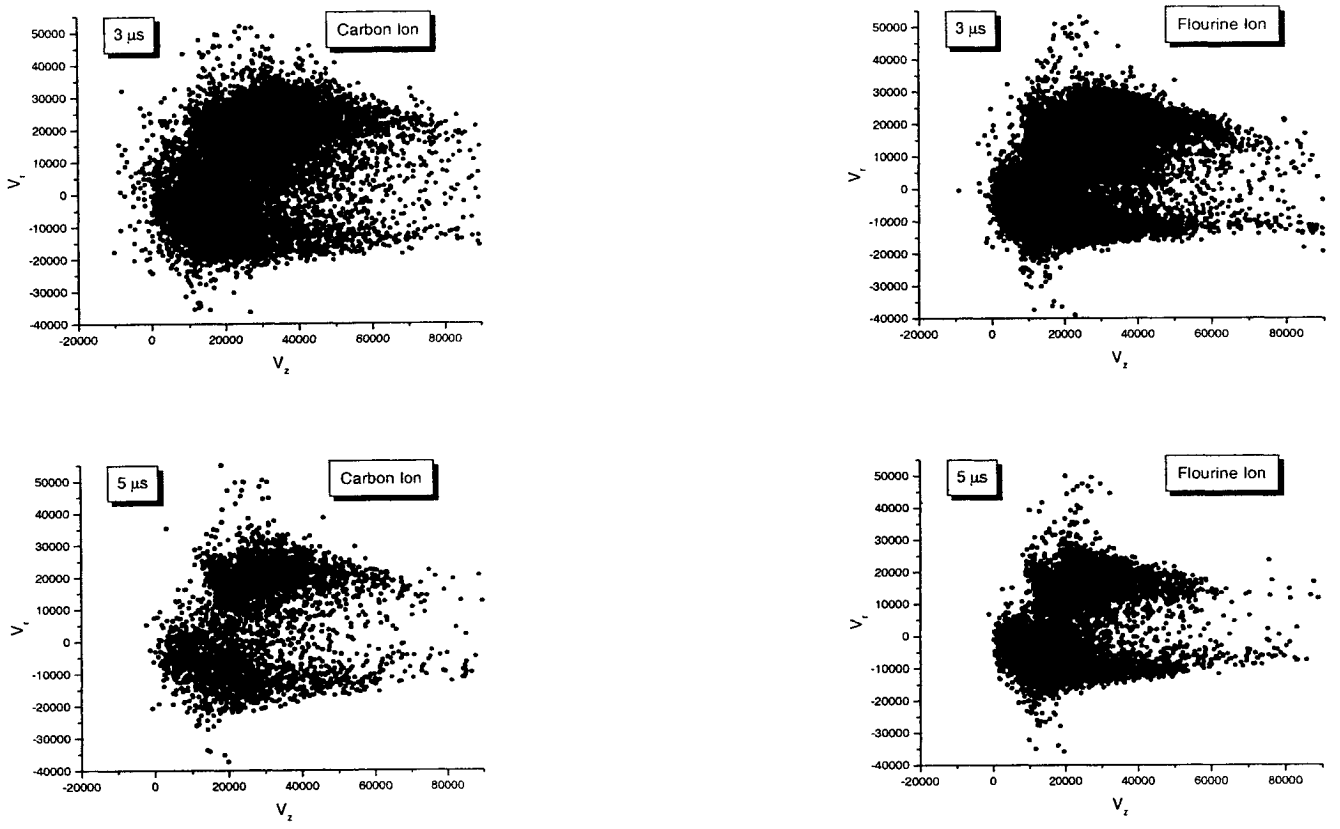

Figure 9. Ion velocity phase. Late stage of the pulse